Materials and Design 97 (2016) 163–174

Contents lists available at ScienceDirect

Materials and Design

journal homepage: www.elsevier.com/locate/matdes

Graphene/poly(ethylene glycol) nanocomposites as studied by molecular dynamics simulations

Roza-Eleftheria Roussou, Kostas Karatasos *

Laboratory of Physical Chemistry, Department of Chemical Engineering, Aristotle University of Thessaloniki, 54124 Thessaloniki, Greece

ARTICLE INFO

Article history:
Received 7 December 2015
Received in revised form 16 February 2016
Accepted 19 February 2016
Available online 22 February 2016

Keywords:
Graphene
Poly(ethylene glycol)
Nanocomposites
Simulations
Structure
Dynamics

ABSTRACT

Fully atomistic molecular dynamics simulations were utilized to examine melt dispersions of graphene nanosheets in a poly(ethylene glycol) (PEG) matrix, in a wide temperature range and for two different polymer sizes. The resulted mixtures were characterized by the organization of graphene in oligomeric clusters. No indications for polymer crystallization were noted in the examined time window. Instead, a weak thermal transition was observed upon cooling, at a temperature higher than the nominal glass transition and the melting point of the polymer. This was found to be associated with the formation of a kinetically-arrested graphene network within the polymeric matrix. Close and below the transition region PEG chains in the composites exhibited frozen-in configurations with an enhanced degree of conformations bearing short end-to-end distances, with those of the higher molecular weight characterized by more distorted shapes close to graphene planes. No polymer intercalation between graphene sheets was observed in the examined samples, while only a weak interaction between the two components was noted. Polymer dynamics in the mixtures were slowed down both in local and in global length scales, accompanied by a distinctly different temperature dependence of the pertinent relaxation rates, compared to those in the pristine macromolecular systems.

1. Introduction

Graphene-based polymer nanocomposites have recently attracted a strong scientific and industrial interest [1–4] towards an effort to fabricate materials with high added value, which combine the advantageous features of the two components. Graphene (GR), being a high aspect ratio filler with enhanced electronic and thermal conductivity [5,6], thermal stability [7–9], gas barrier behavior [10,11] and mechanical properties [7,12,13], appears as a highly promising additive for the improvement of the overall performance of the host polymeric component. In general, the physical properties of such mixed systems were found to depend on several parameters, among others on the characteristics of the dispersion of the GR layers and the nature of the interactions between GR and the polymeric matrix [1,14,15], the amount of wrinkling in the GR [15], the polymer architecture [16,17] and the sample preparation procedure [1,5].

One of the most extensively examined polymers acting as the host matrix for composite materials based on carbon nanofillers [14,18–23], is poly(ethylene oxide) (PEO), due to its high technological importance in areas such as biomedicine [24,25], polymer-based electrolytes [26–28], fuel cells [29] and smart materials (phase switching components) [30,31]. For the production of PEO/graphite-based nanocomposites several protocols have been developed [14,32–34] which resulted in systems appropriate for a wide range of novel applications [18,21,29,32]. Among them, melt blending appears as a cost-effective and scalable procedure [35–37] which may offer a faster route towards the industrialization of the production and thus the commercialization of such materials. Apart from their technological importance, PEO/graphite-based composites have also been utilized as model systems for a more detailed examination of the microscopic mechanisms which are ultimately responsible for the manifestation of the macroscopic behavior of this class of polymer/filler materials.

Along these lines recent studies have focused on the effects of the presence of the filler (in most cases graphite oxide) on the thermal properties [9,38], the structural characteristics [19,39,40] and the dynamics [23,40] of the polymeric component. In these and other studies it was demonstrated that the presence of the graphite-based filler (reduced GR, or graphite oxide) resulted in a shift to lower temperatures of observables such as the glass transition and the melting point of PEO [21,22,34,40]. In some of these works which focused on the examination of local PEO dynamics [19,23] and the interactions between PEO and the graphite-based filler [22,34,40], a correlation between the conformational changes and the mobility of polymer chains near the polymer/filler interface, and the thermal response of the polymeric phase was conjectured. In other recent studies [41], the degree of physical adsorption of non-conjugated polymers, such as PEO, onto chemically reduced GR was found to depend on the molecular weight of PEO, particularly in the low molecular weight range (between 200 and 1500 g/mol). This is exactly the range within which a steep change of

* Corresponding author.
E-mail address: karatas@eng.auth.gr (K. Karatasos).

http://dx.doi.org/10.1016/j.matdes.2016.02.078
0264-1275/

the melting temperature of PEO as a function of molecular weight in the bulk takes place [42,43].

To obtain a more detailed microscopic view on issues related to the spatial arrangement of the two components in the composites, to the conformational features and the dynamics of the polymer in the presence of the filler, to possible effects of polymer molecular weight and of temperature in these characteristics, we have performed fully atomistic molecular dynamics simulations of GR nanosheets dispersed in low molecular weight fragments of PEO, i.e., poly(ethylene glycol) (PEG), in a wide temperature range. We have opted in studying mixtures mimicking the melt-blending procedure without a chemical modification of GR or covalent attachment between the two constituents, in order to describe systems without any potentially destructive effects [44] in the desirable properties of the two components. To better assess the effects of the presence of GR in the behavior of PEG, we have compared our findings to results from analogous simulations of the corresponding pristine polymers. To our knowledge, this is the first attempt of examining multi-GR/multi-PEG chain mixtures in full atomistic detail and in a temperature range spanning 400°.

2. Description of the models and simulation methodology

Two models of PEG/GR mixtures and two systems containing only polymer chains with molecular weights corresponding to those in the composite systems, were simulated in temperatures varying between 300 K–700 K. In the PEG/GR models the volume fraction of GR was kept constant to approximately 22%. We have chosen to study systems with a rather high loading in GR, in order to consider composites with a high degree of reinforcement of the polymer's properties [45,46]. In such systems we can also anticipate more pronounced effects, related to the increased amount of polymer/GR contacts, in the conformational characteristics and the dynamic properties of the polymeric component while also improving the statistical reliability of the analysis associated with the behavior of polymer chains close to graphene. We have examined two different sizes of PEG chains with one about double than the other, namely 855 g/mol (19 monomers) and 1736 g/mol (39 monomers), both lying below the entanglement limit [47], mixed with the same number of GR nanosheets bearing lateral dimensions comparable to the average size of the polymeric constituents, i.e., 15 Å × 15 Å. Details of the examined systems are provided in Table 1.

Forcefield parameters for the linear polymers of the mixtures were taken from the AMBER forcefield [48] which has been shown to be appropriate for the description of fully atomistic models of PEO in different thermodynamic environments [49–51]. Validation of the used parameter set for the pristine PEG models was provided via comparison to available pressure-volume-temperature (PVT) data (see Section 3.1), the characteristic ratio of the chains (see Section 3.2) and the solubility parameters of the polymer (see Section A in supplementary material). Bonded and non-bonded interactions for GR were also modeled using the AMBER forcefield parameters for generic aromatic carbon atoms, on account of recent fully atomistic molecular dynamics simulations which examined properties of pristine GR [52–54] and complexes of GR with other polymeric components [17,55–57]. No special constraints were imposed to keep the GR flakes perfectly planar. Fig. 1 provides a graphical representation of a GR sheet together with a repeat unit of ethylene glycol as used in our study.

Table 1
Details on the composition of the examined systems.

Systems' notation	Number of polymer chains	Number of GR sheets	Volume fraction of GR at 300 K (*v*/*v* %)
20peo39	20	0	0
20peo39g	20	20	22.1
40peo19	40	0	0
40peo19g	40	20	22.3

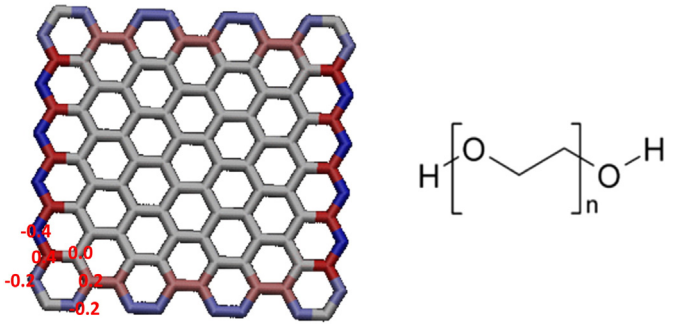

Fig. 1. (Left) A graphical representation of a GR nanosheet used in the model mixtures. The carbon atoms are represented as rods. Partial charges in |*e*| assigned to the edge carbons are also displayed, following Ref. [60]. (Right) A PEG monomer as used in the present study.

The construction of the initial configurations both for the systems with the pristine polymers and those with the GR inclusions, was performed by utilizing the open-source package Packmol [58], in boxes corresponding to densities expected for room temperature conditions. The polymer chain models were taken from our previous work [51] by appropriately adjusting the molecular weight per chain, while the GR nanosheets were constructed by the aid of the VMD package [59]. Ensuing the construction of the initial configurations, the systems were subjected to energy minimization in order to reduce possible close contacts. Those models were taken as initial inputs for an annealing procedure comprised by combined isobaric-isothermal (NPT) MD simulations and further steepest descent and conjugate gradient energy minimization cycles at each temperature.

Starting from a temperature of 300 K and increasing it by steps of 50 K until a temperature of 700 K was reached, each model was equilibrated as described above for several tens of ns depending on the temperature and the system under examination. For all systems the collection of data was performed during the cooling procedure from 700 K down to 300 K, also with 50 K steps. The last frame at each temperature served as the initial configuration for the equilibration procedure targeting the immediately lower temperature. Again, at each temperature during the cooling process, energy minimization as well as several tens of ns of NPT MD runs were performed prior to the commencement of the production trajectories, so that characteristic energetic, static and thermodynamic properties of the systems (total energy, specific volume, average size of the polymer molecules and spatial arrangement of the two components in mixtures) were stabilized within the duration of the equilibration period; at the end of this procedure polymer chains have diffused at distances several times longer than their average size (as the latter is expressed by their radius of gyration).

In the MD productions runs a timestep of 1 fs was used in conjunction with a velocity Verlet algorithm, with a saving frequency of 1 ps. Pressure was kept at 1 bar by means of the Nose-Hoover Langevin piston method [61] (using a piston period of 0.1 ps and a decay time of 0.05 ps) while temperature was controlled with the Langevin algorithm (using a damping coefficient of 3 ps^{-1}). For the computation of electrostatic interactions the particle mesh Ewald (PME) scheme was employed [62]. All simulations were performed with NAMD 2.9 [63] using periodic boundary conditions and with a cutoff of the Van der Waals interactions at 12 Å (a switching function was also employed at the last 2 Å to avoid discontinuities in the potential and the forces). Fig. 2 shows an example of the result of the equilibration procedure followed, for the composite systems.

After equilibration, there was a departure of the graphene geometry from a perfectly-flat plane. Our calculations showed that the degree of shrinkage in the lateral dimensions of the graphene sheets remained

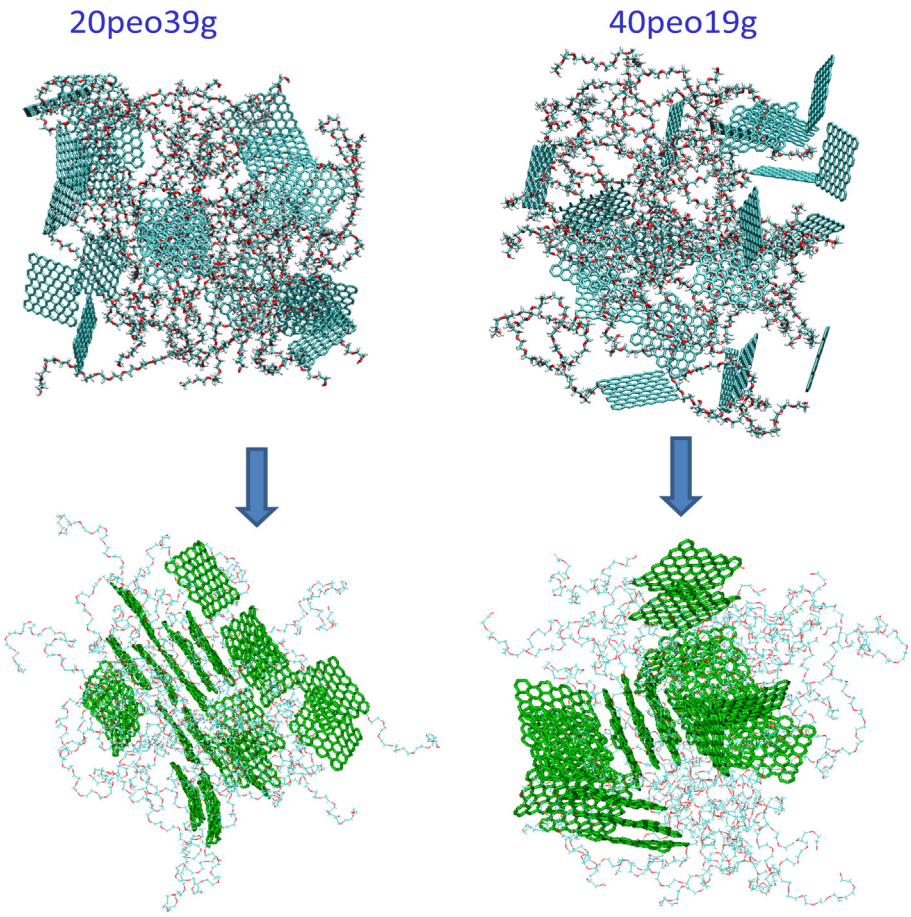

Fig. 2. Initial (upper part) configurations, just after construction, and final (lower part), configurations prior to the commencement of the production runs for the two composite systems at 600 K. In the equilibrated snapshots, GR flakes are shown in more intense color while only the backbone of the linear chains is depicted, in order to highlight the dispersion of the GR flakes in the polymeric matrix.

below 4% with respect to the corresponding unperturbed dimensions at all temperatures and for both the composite models. To describe a GR plane, we have considered that it could be represented to a good approximation via the plane defined by the two principal axes of inertia of the platelet which are on average parallel to the GR's surface; the direction of the platelet was then defined by the third axis which completes the orthogonal system of the principal axes of inertia.

3. Results and discussion

3.1. Thermal response of the systems

As quoted in past studies of the thermal behavior of pristine PEO melts [64], short chains will tend to form metastable folded-chain structures when subjected to fast cooling rates, rather than forming extended

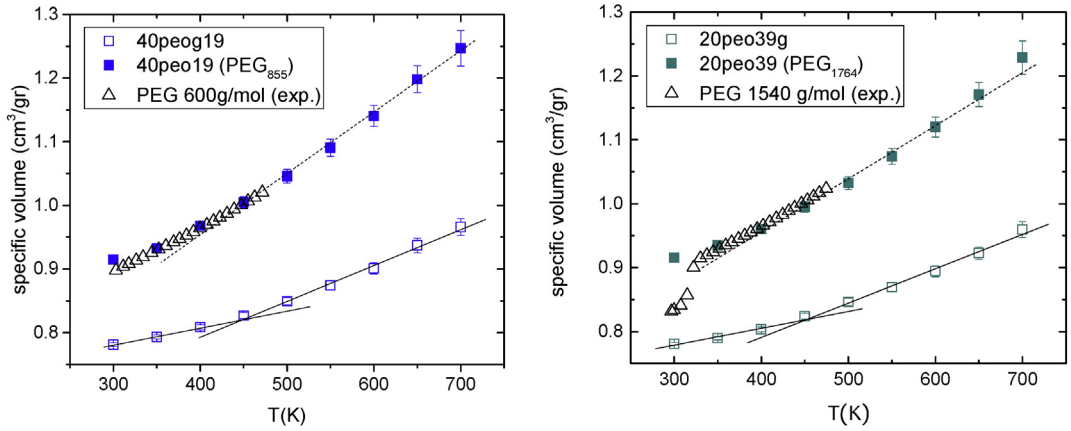

Fig. 3. Temperature dependence of the low (left) and the high (right) molecular weight PEG-based systems. Open triangles correspond to experimental PVT data [70] of PEG melts bearing chains with molecular weights comparable to those simulated. The dashed lines are linear fits to the high-temperature behavior of the simulation data of the pristine polymers, while the solid lines are fits to the high and lower-temperature behavior of the specific volume in the composite systems.

crystalline domains. In addition, at high cooling rates the crystallization is anticipated to shift to lower temperatures [65–67]. Our models essentially mimic this situation, since we are examining low molecular weight PEO chains while the usual effective cooling rate in MD simulations is high [68,69] (typically of the order of 10 [9] K/s, as in our case).

The melting temperatures for actual polymer bearing molecular weights of Mw = 855 g/mol and Mw = 1736 g/mol were estimated [42] to be 309 K and 326 K respectively (the authors of Ref. [42] quote that the corresponding crystallization temperatures differ by less than 10° from melting points for low molecular weight PEO fragments). These values are very close to the melting temperatures of 306 K and 321 K determined for PEG chains of Mw = 890 g/mol and Mw = 2120 g/mol respectively, from Ref. [43]. The glass transition temperatures for the examined PEG chains lie several tens of degrees below 0 °C [42,43].

Fig. 3 depicts the temperature dependence of the specific volume of the examined systems. The straight lines are linear fits to the simulation data, while open triangles show available experimental points from PEG melts with molecular weights close to the simulated polymeric chains [70]. Focusing on the pristine polymers' behavior, it appears that simulation data are in good agreement with the experimental points (with the exception of the point corresponding to the lower examined temperature, i.e., 300 K), despite the fact that the experimental measurements were conducted with a rather low cooling rate (less than 5°/min as noted in Ref. [70]) and the experimental molecular weights are somewhat lower. In both systems a deviation between the high and the low-temperature behavior can be observed, which, based on a simple statistical analysis (see Figs. S2–S5 in supplementary material) seems to be present also in the experimental data.

The experimental behavior might be related to a metastable state of chain reorganization upon approaching the nominal crystallization temperature [71–73]. The high molecular weight experimental data exhibit a sudden drop at temperatures below ~320 K which denotes the onset of crystallization [67,74]. However, no such drop is observed in the corresponding simulation data. This most probably can be attributed to the higher effective cooling rate in which the simulated chains are subjected as noted earlier, which results to a supercooling of the polymer melt that shifts the crystallization to a lower temperature compared to the melting point [67]. On the other hand the behavior of the two nanocomposites is very similar. They also exhibit a change in slope of the specific volume with respect to the high temperature behavior in a similar temperature range, which is more pronounced in comparison to the pristine polymer systems. It is reasonable, therefore, to consider that the presence of GR affects the organization and/or the kinetics of the polymer chains, suppressing any abrupt change in the system's density that would be indicative of a crystallization transition, under the examined conditions. This picture is consistent with previous findings in polymer/nanofiller composites, where it was demonstrated that an increased concentration of nanofiller incurs a retardation of the crystallization kinetics resulting to a lower degree of crystallinity compared to that of the pristine polymer [46,75,76].

The observed changes in the temperature dependence of the specific volume between the composites and the pristine polymers, can be directly linked to differences in the anticipated thermal stability of the systems by examining the respective thermal expansion coefficients defined as

$$\alpha = \frac{1}{v_s}\left(\frac{\partial v_s}{\partial T}\right)_P \tag{1}$$

where v_s represents the specific volume. Based on the slopes appearing in Fig. 3 and in Figs. S2 and S4 in the supplementary material for the high (HT) and the low temperature (LT) regimes and the values of v_s corresponding to the high temperature onset of each regime, we have calculated the values of α as listed in Table 2.

Table 2
Thermal expansion coefficients for the examined systems.

System	α (K^{-1}) HT	α (K^{-1}) LT
PEG 600	7.9	6.9
40peo19g	5.6	3.3
PEG 1540	7.9	7.3
20peo39g	5.3	2.7

Comparison between the thermal expansion coefficients corresponding to the nanocomposites and to the close in PEG molecular weight pristine samples, reveals that in both regimes and for systems of both PEG molecular weights, the thermal expansion coefficient is lower in the graphene nanocomposites. The values of α appear to be approximately 30% lower in the nanocomposites in the HT regime and more than two times lower in the LT regime, compared to the pure polymers. This behavior implies a significant improvement in the thermal stability of the nanocomposites over that of the pristine polymers.

To gain a better insight on the changes imparted by the presence of GR and by the temperature decrease, we have monitored pertinent properties both on system-wide as well as on local length scales as described in the next sections.

3.2. Chain conformational characteristics

To check whether the presence of GR affects the conformational features of the polymer chains, we have compared the characteristic ratio of PEG molecules in the pristine state and in the composites, as shown in Fig. 4. The characteristic ratio C_n is defined as

$$c_n = \frac{\left\langle R^2_{e-e}\right\rangle}{nl^2} \tag{2}$$

where $\langle R^2_{e-e}\rangle$ corresponds to the mean-square end-to-end distance of the polymer chain (time and ensemble average), n is the number of main-chain backbone bonds and l the mean length per skeletal bond (the denominator essentially describes the average mean-square length of a freely jointed chain).

For the pristine polymer systems as well as for the composite comprised by the shorter PEG chains, the characteristic ratio remains very close to a value of 5 throughout the temperature range examined, within the error margins, which is in reasonable agreement with experimentally measured values for PEO oligomers of 4.8 ± 0.4 [77], and with values for higher molecular weights ranging between 5.3 and 5.9 [78,79]. In the composite formed by the higher molecular weight PEG chains (Fig. 4, left), it appears that at temperatures below 450 K, the characteristic ratio assumes moderately lower values.

A lower value of C_n would be consistent either with a more flexible polymer backbone, or with the existence of chain configurations where the two chain ends can be found within a relatively short distance. Since there is no obvious reason for the longer PEG chains to become more flexible as the temperature drops, it should therefore be anticipated that upon decrease of temperature the population of chain configurations with a short end-to-end distance must be increasing on average. This can be confirmed by examining the distributions of the end-to-end distance of the polymer chains, as they are presented in Fig. 5.

For all models, the chain end-to-end distance assumes a Gaussian shape at the high temperature regime (as this is defined in Fig. 3). At the lower temperature regime multiple peaks appear, indicating the development of frozen-in configurations. When comparing Fig. 5a to b and c to d, it appears that the deviation of the distributions from Gaussians takes place at higher temperatures in the nanocomposites (i.e., at 400 K for Fig. 5a compared to 500 K in Fig. 5b and at 450 K in Fig. 5c compared to 550 K in Fig. 5d). In addition, at the lower temperature regime,

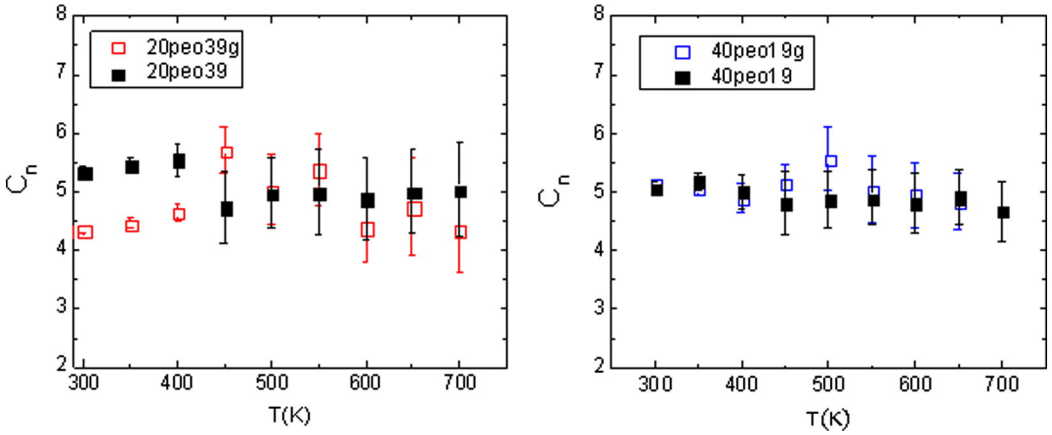

Fig. 4. Characteristic ratio of the long (left) and the short (right) length PEG models.

the PEG chains in the nanocomposites exhibit a higher propensity of configurations with shorter end-to-end distances compared to the behavior in the corresponding pristine PEG. This notion can be quantified by estimating the percentage of chains with end-to-end separation considerably smaller than the average end-to-end distance. To extract statistically reliable estimates we considered all polymer configurations bearing end-to-end distances smaller than half of the corresponding average end-to-end separation. The results are presented in Table 3.

As shown in Table 3 the percentage of chains bearing a short separation between the chain ends grows significantly in the composite systems. The same trend is present if we select a different cutoff within the aforementioned criteria (see Table S1 in the supplementary material). An analogous calculation as above, regarding the percentages of chains assuming conformations with end-to-end distances 50% larger than the average end-to-end separation of the polymer chains, did not show any specific trend towards an increase or decrease of the relative percentages in the presence of GR, while no systematic differences were observed when comparing the composite systems with different polymer molecular weights (see Table S2 in the supplementary material). In the infrequent instances where such extended conformations were detected in the composite systems, they haven't been found to be associated with intercalation of the polymer chains between parallel (or almost parallel) graphene flakes.

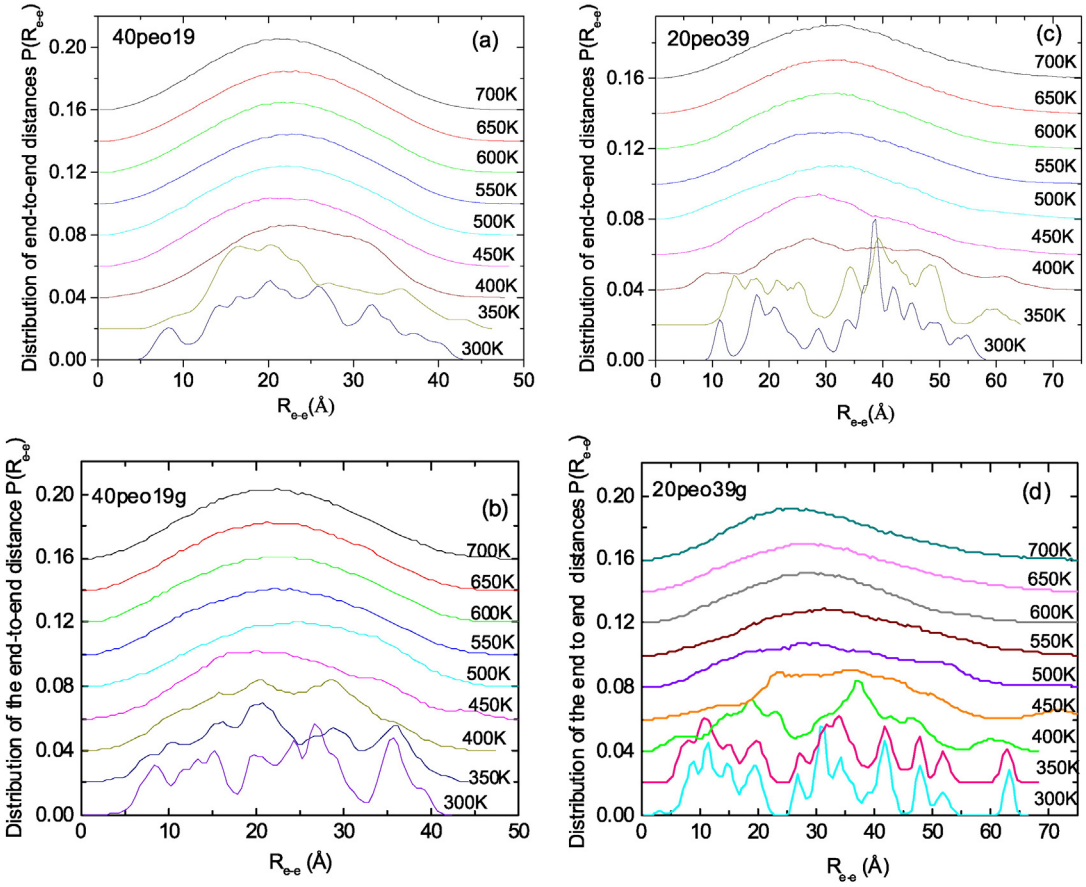

Fig. 5. Distributions of the end-to-end distances of the polymer chains in the short-PEG (left, a, b) and long PEG systems (right, c, d). Each curve is shifted by 0.2 in the y-axes with respect to its immediately lower curve for clarity.

Table 3
Comparison of the percentage of chains assuming configurations with end-to-end separation less than half of the average end-to-end distance of the polymer chains, at low temperatures.

System\temperature	$T = 400$ K	$T = 350$ K	$T = 300$ K
20peo39	11.7%	15.4%	12.7%
20peo39g	16.4.%	28.8%	28.5%
40peo19	9.0%	5.1%	8.5%
40peo19g	12.2%	13.4%	15.3%

3.3. Spatial arrangement of the components in the mixture

The observed changes on chain configurations in the nanocomposites, could be closely related to the specifics of their dispersion in a mixture with a filler possessing a highly anisotropic shape [80,81]. To monitor the polymer's arrangement in the mixtures and compare it with that in the pristine PEG systems, we have calculated the radial distribution functions arising from the centers of mass of the polymer chains, as illustrated in Fig. 6.

A visual inspection of the pair correlation functions in the pristine systems and in the composites shows that at the high temperature regime no significant differences are observed. This indicates that despite the presence of GR, when sufficient kinetic energy is provided by means of the elevated temperature, the ability of polymer chains to rearrange is not affected significantly by the filler, allowing thus a similar spatial arrangement with that realized in the bulk polymer samples. On the other hand, as temperature lowers significant deviations are building up, indicating that the presence of GR intervenes in a decisive manner to the polymer kinetics and therefore in the final pseudo-equilibrium polymer configuration.

At the lower temperature regime, the formation of distinct peaks implies the gradual localization of the polymer chains at characteristic relative distances. This behavior is more prominent in the composite systems (notice the differences in the number, the sharpness and the relative intensity of the peaks from the corresponding spectra of the pristine systems). It is also worth noticing that in the composite systems comprised by the double in size chains (Fig. 6, left), significant deviations from the pertinent pristine polymer's behavior appear at higher temperatures (i.e., at 500 K), compared to that of the short PEG systems (i.e., 450 K, Fig. 6, right). These observations can be directly correlated with the behavior described in Section 3.2 regarding the changes observed in the polymer conformations at the different temperature regimes.

The increased localization of polymer chains at lower temperatures in the composite systems, should naturally be related to the topological constraints imposed by the GR flakes. The development of the GR-related structure in the composite systems is presented in Fig. 7, where the radial distribution functions arising from the center of mass of GR sheets are presented as a function of temperature.

For both composites the radial distribution functions at the higher temperatures are reminiscent of a liquid-like structure. As the temperature decreases we observe the development of several peaks which grow in number and in amplitude, particularly when the systems enter the low temperature regime, suggesting the establishment of a structure which becomes fixed in space. The formation of such a structural pattern of the GR dispersion upon lowering the temperature, provides the context within which the behavior of the polymer chains described in Fig. 6 for the composite systems can be easily understood.

A visualization of the polymer/GR dispersions in the composites is provided in Fig. 8 at the lowest examined temperature and at a temperature close to the change in slope of the specific volume (see Fig. 3). A cursory glance in the snapshots of Fig. 8 reveals that the preferable organization of GR is in oligomeric clusters which are dispersed within the polymer matrix (see also Fig. S6 in the supplementary material). This behavior was also noted in experimental studies of polymer/GR composite systems [45,82,83]. The absence of an appreciable degree of PEO intercalation between stacked GR sheets is consistent with X-ray diffraction data in GR/PEO nanocomposites [34,40] where no intercalated structures were observed, in contrast with analogous measurements in graphite oxide/PEO mixtures where PEO intercalation within graphite oxide platelets was clearly detected [9,19,21,39].

3.4. Packing and shape of the polymer chains in the composites

One of the key parameters which was found to affect considerably the characteristics of the polymer/filler dispersion is the strength of the interactions close to the interfacial region [1,20,38,84–87].

Particularly in the case where the polymer phase is crystallizable, this parameter essentially controls the ability of the filler particles to act as nucleation sites [1,75,88–90] in the crystallization process. Recent studies in GR/polymer nanocomposites in which the polymeric component was crystallizable, verified that the first stage towards this process

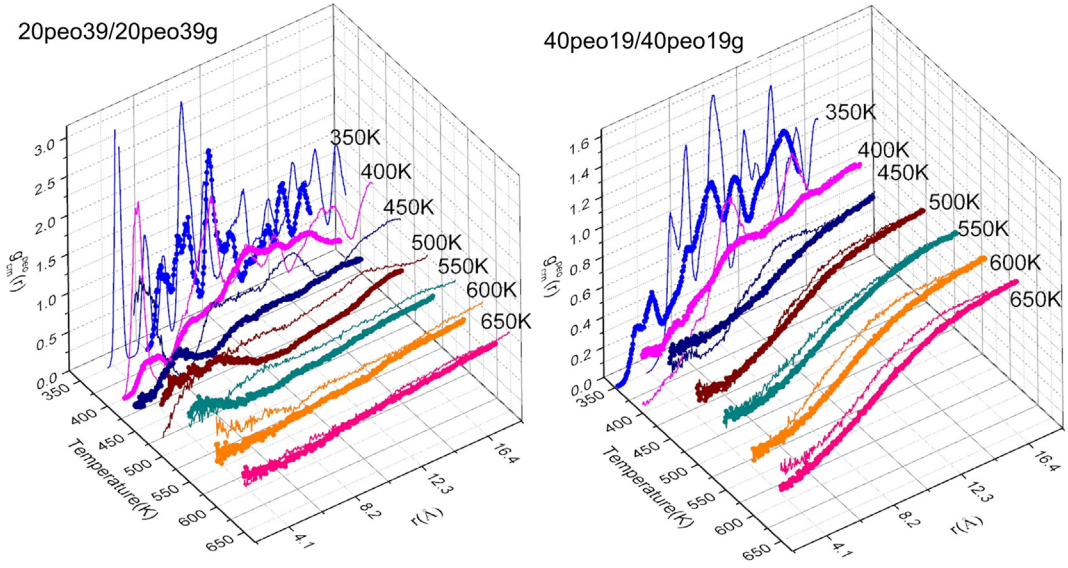

Fig. 6. Comparison of radial distribution functions of the centers of mass of the PEG chains in the pristine systems (symbols) and in the nanocomposites (lines). The 700 K data are not included due to the overlap between the respective curves, while those of 300 K are not shown for clarity.

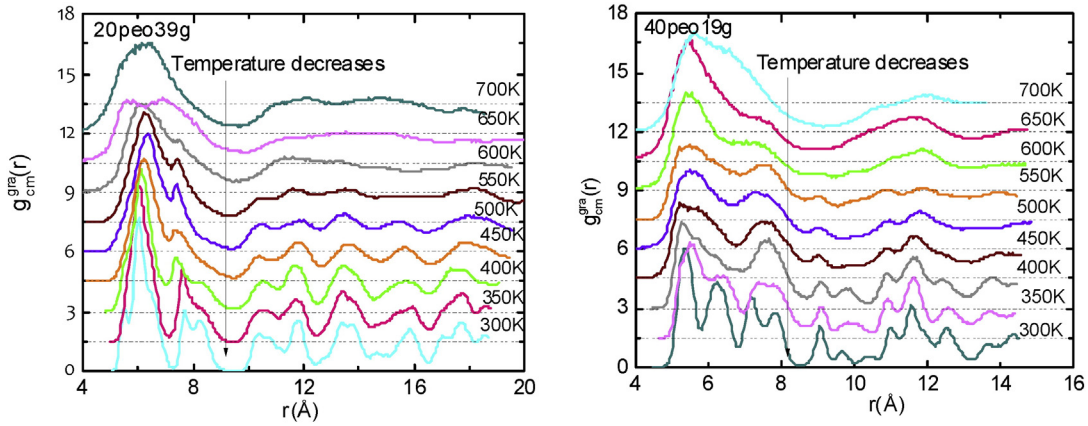

Fig. 7. Temperature dependence of the radial distribution functions arising from the center of masses of the GR flakes for the shorter PEG-based (right) and the longer PEG based (left) systems. Each curve is shifted by 1.5 with respect to its previous in the y-axis for clarity.

was the physical adsorption of the polymer chains onto GR's surface [89, 91–93], followed by the diffusion-controlled growth of the crystalline lamellar structure.

To check the degree of physical adsorption of PEG chains onto GR, we have constructed the polymer density profiles in a direction normal to the GR's plane. These are presented in Fig. 9. In both composites the profiles are characterized by a peak close to a distance of 4 Å which is followed by additional peaks at longer distances from the GR's surface.

The peak at the shortest distance can be assigned to the polymer layer closest to the GR plane, while those at longer distances can be attributed to the polymer layers close to neighboring GR flakes, such as those belonging in the same or in neighboring clusters (see Fig. 8). The number and the location of the peaks characterizing the two models are different, reflecting the differences in the dispersion of the GR clusters in the two systems (see Fig. 7). A common characteristic of both models is that upon the decrease of temperature the intensity of the peaks increases, implying a higher localization of the polymer chains close to the GR particles. This observation is consistent with the gradual freezing-in of chain configurations and polymer localization upon decrease of temperature as was noted in Figs. 5 and 6, in conjunction with the progressive consolidation of the graphenes' structural pattern as described in Fig. 7.

Another feature common in the behavior of the two composites is the rather low intensity of the peaks; this is in stark contrast with the high local density of PEO close to a strongly interacting surface [94], which implies only a weak interaction between PEG chains and GR. The same conclusion can be drawn when examining the profiles of strongly adsorbing chains onto GR, which exhibit sharper and much

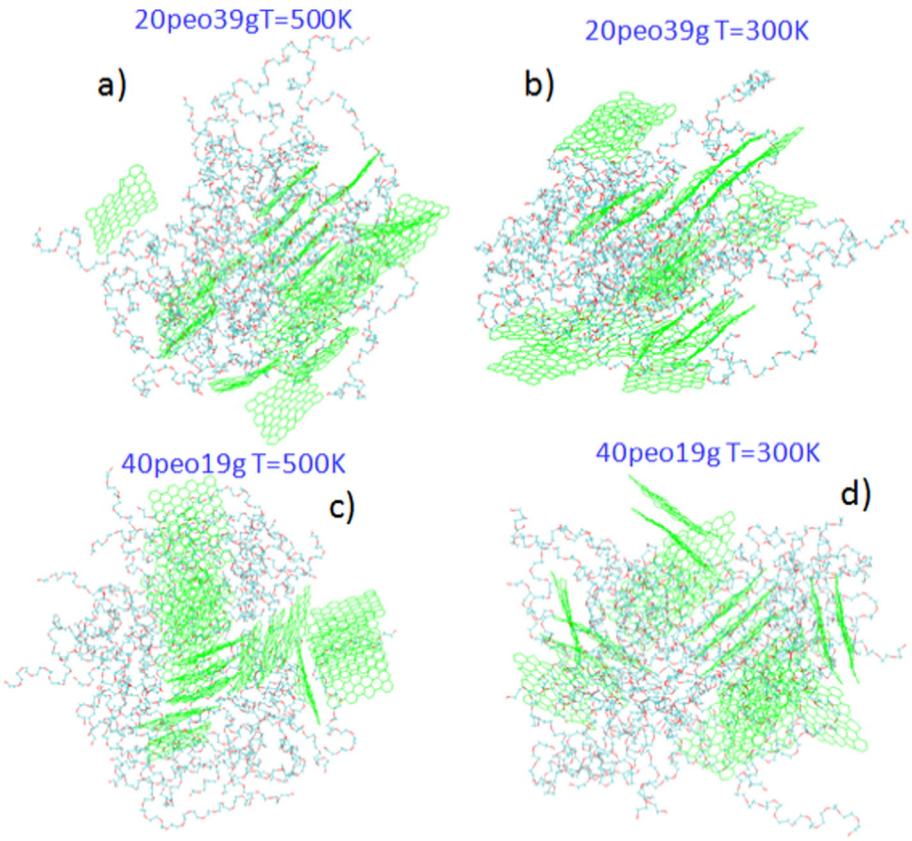

Fig. 8. Snapshots of the longer (a, b) and the shorter (c, d) PEG- based composites, at temperatures of 500 K and 300 K. The polymer chains are represented only by their backbones.

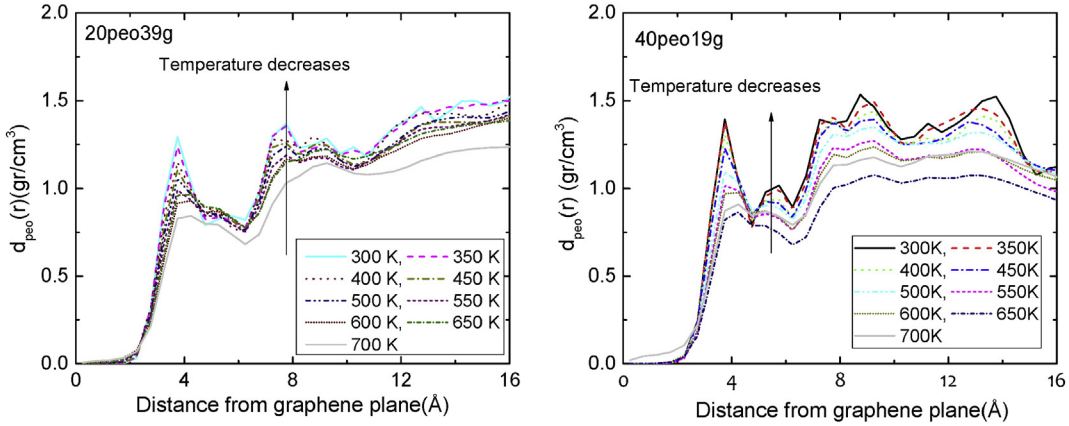

Fig. 9. Symmetrized polymer density profiles as a function of the distance from a GR's plane.

more intense peaks close to GR's surface, reaching local densities several times higher than that of the bulk polymer away from the surface [86,91–93,95]. In previous studies where a rather weak interaction between PEG and graphite oxide was found, this was accompanied by a lower degree of crystallinity compared to the pristine polymer [21,34], while for strongly interacting polymers with graphite oxide particles [76,96] or GR [97], an increased degree of crystallinity was detected during isothermal crystallization.

Previous studies examining the geometric characteristics of polymer chains near strongly interacting flat surfaces (including GR), showed a significant degree of distortion to their shape [98–102]. Even in cases of weak, or no favorable polymer/surface interactions, a certain degree of elongation and/or flattening of the chains located adjacent to the surface, was noted [85,103,104]. Therefore, even in the case of the examined systems where only weak interactions between PEG chains and GR are supported by the data, such distortions to the shape of chains close to a GR surface might be present. To check this hypothesis we have calculated the average length of the diameters of the ellipsoid of inertia of a polymer chain, as a function of the distance between the center of mass of the chain and a GR particle. In this calculation we have considered all chains for which their center of mass lie within the volume of a parallelepiped having as base the graphene plane and extending bilaterally along a direction perpendicular to it. The results for the longest diameter of the ellipsoid of inertia for those polymer chains are presented in Fig. 10.

Comparing the systems with the different PEG sizes, it appears that the chains in the shorter PEG system do not show any significant trend towards elongated conformations close to GR platelets. This insensitivity in shape of the short chains close to a GR plane holds true for the other two diameters of the ellipsoid of inertia as well (see Fig. S7 the supplementary material). This is not the case, however, for the longer PEG system, where a clear trend towards more elongated shapes close to a GR platelet is observed, particularly as temperature decreases. At the same time, the shape of the ellipsoid of inertia of chains close to a GR surface becomes somewhat distorted in the other directions, as well (see Fig. S7 in the supplementary material). Therefore, it appears that the propensity for shape distortions of PEG chains close to a weakly interacting GR surface correlates directly with the size of the chain, in line with a configurational-entropy-driven scenario in the absence of strong interfacial interactions, as described in past studies for other polymer composite systems [103,104].

3.5. Dynamic response of polymers in global and local length scales

The gradual solidification of the structural pattern formed by the GR platelets as temperature drops, imposes global topological constraints to the chain translational and rotational motion which is expected to result in an overall slowing-down of polymer dynamics at the entire molecular scale [105]. To illustrate this effect in our models, we have monitored the decay rate of characteristic time correlation functions probing global motion.

Fig. 11 compares the overall rotational motion of PEG chains in the pristine systems and in the corresponding composites, as probed by the reorientation of unit vectors $\hat{h}(t)$ which connect the center of mass of a chain with its atoms, according to Eq. (3).

$$C(t) = \frac{1}{2}\left\langle 3\left[\hat{h}(t)\cdot\hat{h}(0)\right]^2 - 1\right\rangle \tag{3}$$

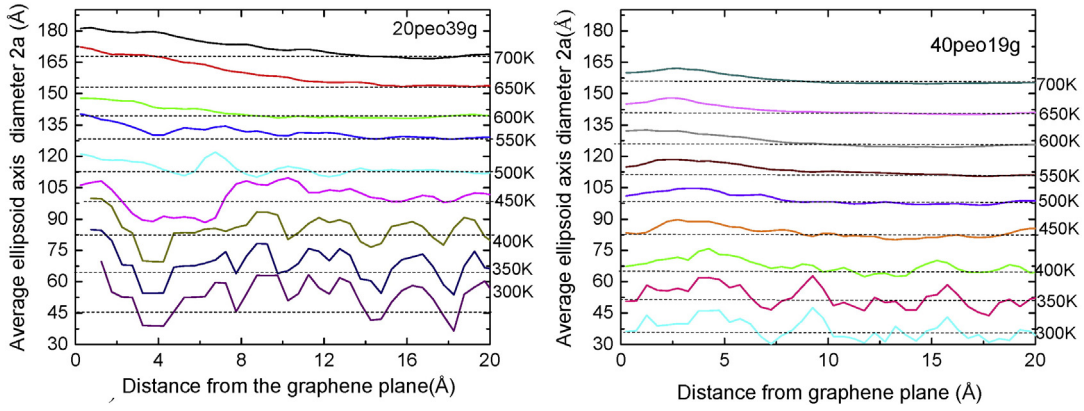

Fig. 10. Average size of the longer diameter of the ellipsoid of inertia of polymer chains, as a function of the separation between the center of mass of a chain and a GR plane. The dashed lines intend to serve as baselines for the behavior of chains away from a GR platelet. Each curve is shifted in y-axis by 15 with respect to its previous for clarity purposes.

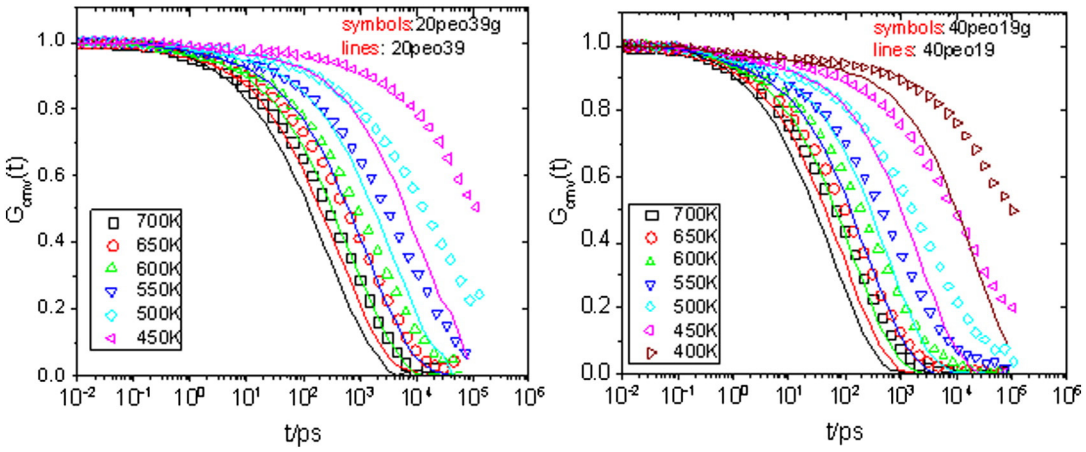

Fig. 11. Comparison of the correlation functions for overall chain rotational motion (Eq. (3)) in the pristine polymer systems (lines) and in the composites (symbols), for the higher (left) and the lower (right) molecular weight PEG models. Same colors in the symbols and the lines denote same temperature.

The angle bracket denotes time and ensemble average. In systems of both polymer sizes, the correlation functions describing the chains in the composites decay at longer timescales compared to those in the pristine polymer models at corresponding temperatures.

By following the behavior of the correlation functions as temperature changes, it can be observed that the difference between the characteristic timescales for the decay of the curves in the pure polymers and those in the composites grows as temperature decreases. A behavior similar to that described by Fig. 11 is also noted for the correlation functions probing the squared fluctuations of the radius of gyration of the polymer chains (i.e., describing the "breathing" motion of the polymer), as shown in Fig. S8 in the supplementary material. The observed slower global polymer dynamics in the composites, in conjunction with the retarded structural relaxation of the PEG chains anticipated close to the interfacial region [94], may also affect the timescale for spatial rearrangements in local length scales (see Ref. [105] and references therein).

To examine the effect of the presence of GR in local PEG dynamics, we have probed the backbone C—C bond reorientational motion by calculating correlation functions analogous to those described by Eq. (3), but this time $\hat{h}(t)$ represents a unit vector along a C—C bond at time t. The results are displayed in Fig. 12.

The slowing down of the bond orientational motion in the composites is apparent when compared to that in the pristine polymers (note the difference in the timescales required for the decay of the corresponding relaxation functions). This slowing down of local PEG dynamics with respect to the pure polymers' behavior should mainly arise from the contribution of monomers in close proximity to a GR flake, since segments away from the filler's surface are expected to behave similarly to those in the bulk [106,107].

In order to quantify the differences in the timescales related to the orientational motion in global and local length scales, we have evaluated the average relaxation times through the analysis based on the distribution of exponential relaxation times [108]. According to this method, each time correlation function C(t) is expressed through a continuous superposition of single exponential relaxation processes which are distributed according to a probability function F, as described in Eq. (4).

$$C(t) = \int_{-\infty}^{\infty} F(\ln\tau) e^{-t/\tau} d\ln\tau \tag{4}$$

Distinct dynamic processes with sufficiently separated timescales, appear as individual peaks in the calculated probability functions [108] (examples of such probability functions are shown in Fig. S8 in the supplementary material). An average relaxation time taking into account all the contributing dynamic processes is then calculated as $\langle\tau\rangle = \int_{-\infty}^{\infty} \tau F(\ln\tau) d\ln\tau$. For a higher reliability in our analysis, we have only taken into account temperatures at which the corresponding correlation functions had relaxed sufficiently (i.e., by at least 80%)

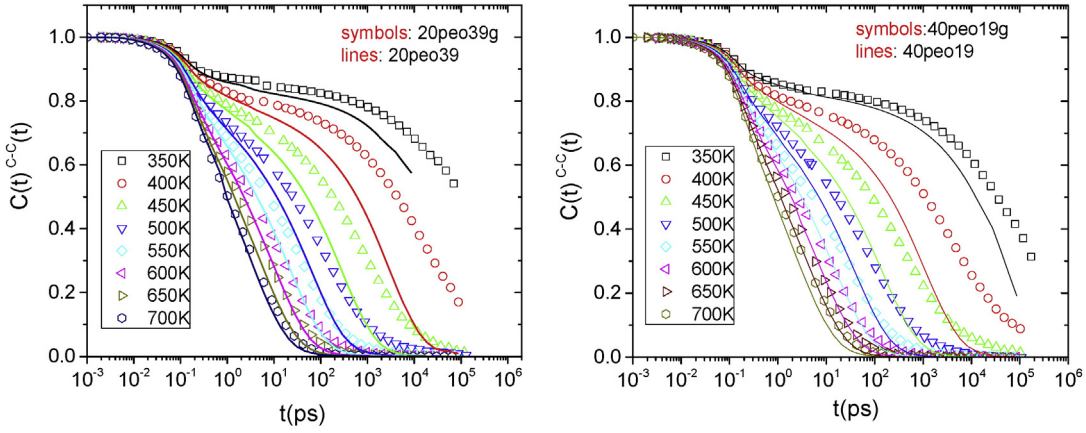

Fig. 12. Time orientational functions of vectors lying along backbone C—C bonds of a polymer chain. Symbols correspond to the behavior in the composites and lines with the same color as the symbols, that in the pristine polymer at the same temperature.

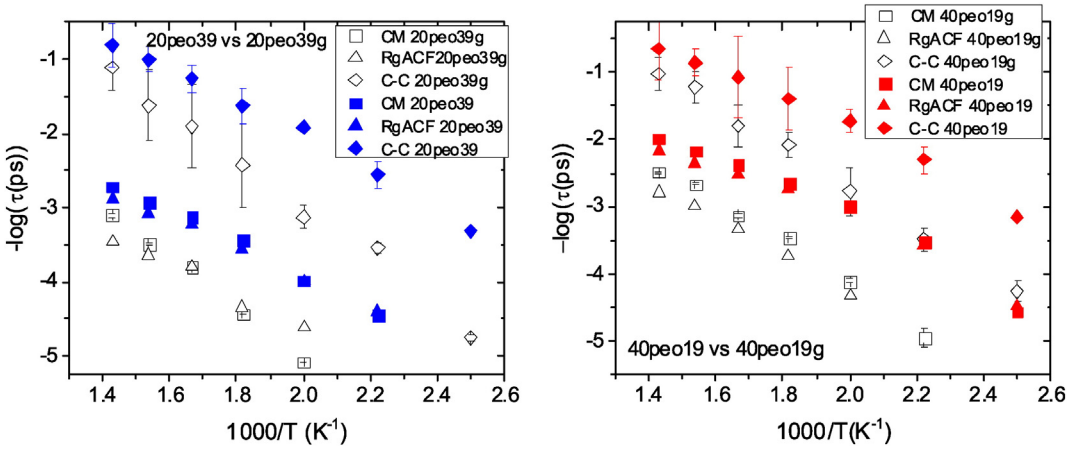

Fig. 13. Average relaxation rates (in logarithmic scale) arising from global and local dynamics (see text) of polymer chains in the composites (open symbols) and in the pristine systems (filled symbols).

within the examined time window. Fig. 13 compares the inverse average relaxation times for global and local dynamics of the examined systems.

In these figures we have also included the relaxation rates arising from the time correlation functions of the fluctuations of the radius of gyration of the polymer chains (see Fig. S9 in the supplementary material). Focusing on the behavior at the entire polymer length scale, it appears that in both systems the overall polymer rotational motion assumes a timescale similar to that describing the fluctuations in size of the chains, indicating a strong coupling between these two relaxational mechanisms, which is manifested in the presence of GR, as well.

Moreover, a key feature common to systems of both polymer sizes, is that the relaxation rates corresponding to the composites (open symbols in Fig. 13) are lower than the respective rates in the pristine polymer systems even at the higher examined temperature, as was visually identified in Figs. 11 and 12. At the high temperature range the separation in relaxation rates between the pristine polymer models and the respective composites is small, but the observed deviations increase significantly as temperature drops, reaching differences of one order of magnitude or larger at the lower temperature regime.

The stronger temperature dependence of the relaxation rates in the composites with respect to the pristine PEG systems, both in local and in global length scales, is indicative of a more cooperative mechanism through which polymer rearrangements take place in the presence of GR. As far as it concerns the behavior at the entire chain length scale, this can be understood in terms of the increasingly sluggish motion of the GR clusters as temperature decreases, which results in the formation of a disordered array of almost immovable obstacles through which polymer chains must rearrange and diffuse [109,110]. On the other hand, the increasing local density close to a GR flake as temperature lowers and the connectivity between the monomers that are weakly adsorbed onto GR, can justify the realization of a more cooperative motion of those polymer segments located close to the surface [105–107,111].

The difference in polymer molecular weight is also reflected in the corresponding relaxation rates, either for global or for local dynamics, where systems bearing the shorter polymer size relax faster. The dependence of polymer dynamics on chain size holds true for the case of composites as well (see Fig. S10 in the supplementary material). Therefore, although the presence of GR results in the slowing down of the dynamics in both local and global length scales, this is done in a manner commensurate to the difference in PEG molecular weights for the examined non-entangled chains. The molecular weight dependence of short scale polymer dynamics is very small when comparison is made between the two pristine polymer models or between the polymers in the composites, due to the local nature of the examined motion.

The observed slowing down of global polymer motion in the presence of graphene, as well as the noticeable change in the respective temperature dependence of the relaxation times with respect to the pure polymers, is expected to have a significant impact on the rheological behavior of such systems (i.e., an increase of the viscosity) since polymer viscosity is directly related to the slowest relaxational modes [112].

4. Conclusions

The aim of this work was to provide new insight regarding the characteristics of melt-prepared composite materials comprised by two different molecular weights of poly(ethylene glycol) and a relatively high loading of graphene nanosheets. To this end we have obtained information associated with the dispersion of the two components in the mixtures, with their thermal response under fast cooling conditions, with the conformational and dynamic properties of the polymeric components in the constricted microenvironment imposed by the presence of GR and with the relative strength of the interaction between the two constituents.

It was found that under the examined conditions, the composites undergo a weak thermal transition at a temperature well above the nominal polymer crystallization point (Fig. 3). The behavior of the specific volume in the composites results in lower thermal expansion coefficients compared to the pristine systems (Table 2), implying an enhanced thermal stability of the nanocomposites. Near the temperature of the weak thermal transition, formation of frozen-in (Figs. 5 and 6) but non-crystalline chain configurations (Figs. 2, 4, 8) is detected, which is associated with the onset of a spatial constriction of the polymer molecules (i.e., a reduced mobility regime, Fig. 11) within an almost solid-like dispersion of GR clusters (Fig. 7).

Based on visual inspection of simulation snapshots (Figs. 2 and 8) and examination of the characteristics of the GR spatial arrangement in the mixtures (Fig. 7), no noticeable degree of polymer intercalation was noted, in line with recent experimental studies of GR/PEO composites [34,40], while no detectable degree of polymer crystallization was noted either.

Near the PEG/GR interface polymer density increased moderately as temperature decreased, indicating a rather weak interaction between the two materials (Fig. 9). In the absence of strong interactions, the observed density modulation of PEG close to the GR surface should therefore reflect the competition between the reduction of configurational entropy of the chains close to the GR plane and the packing constraints imposed by the chains located at longer distances from the GR particles [85].

The presence of the graphene sheets in combination with the absence of strong interactions between the two components, appeared to result in an increase of the percentage of polymer configurations with short end-to-end distance. Only in the composite with the longer PEG chains, and at the lower temperature regime did an elongation of polymer chains close to the GR surface take place (Fig. 10). Based on the behavior known from relevant studies, it is possible that the formation of extended conformations of the longer chains near the GR platelets signifies the onset of a metastable pre-crystallization state [72,73,89]. Development of this state near to the graphene surface at temperatures well above the polymer melting, might affect considerably the local stresses of the neighboring polymer chains, contributing thus to the improvement of the mechanical properties of the composites [113].

A slowing down of polymer motion with respect to the pristine systems in global and in local scale was observed in composites of both polymer sizes as temperature decreased (Figs. 11 and 12). This is consistent with the experimentally detected shift in the crystallization/melting temperature of such mixtures with respect to pure polymers [21,22,34,40]. The degree of slowing down in the entire chain length scale in the composites, appeared to scale with molecular weight in a manner similar to that in the pristine polymer systems (Fig. 13). This should probably be related to the fact that both molecular weights lie below the chain entanglement limit. The remarkable change in the temperature dependence of the average relaxation rates with respect to the pristine polymers' behavior, was consistent with an increased degree of cooperativity both in local and global length scales, induced by the presence of GR.

Although the above findings refer to mixtures of GR with a specific polymer, we believe that they may serve as the basis for the interpretation of the behavior and the optimization of properties of other nanocomposites based on GR and weakly-interacting non-entangled crystallizable polymers.

Acknowledgments

This research has been co-financed by the European Union (European Social Fund — ESF) and Greek national funds through the Operational Program "Education and Lifelong Learning" of the National Strategic Reference Framework (NSRF) — Research Funding Program: Thales. Investing in knowledge society through the European Social Fund (MIS 377278).

Appendix A. Supplementary data

Supplementary data to this article can be found online at http://dx.doi.org/10.1016/j.matdes.2016.02.078.

References

[1] H. Kim, A.A. Abdala, C.W. Macosko, Macromolecules 43 (2010) 6515–6530.
[2] A.K. Geim, K.S. Novoselov, Nat. Mater. 6 (2007) 183–191.
[3] A.M.K. Esawi, M.M. Farag, Mater. Des. 28 (2007) 2394–2401.
[4] M.M. Shokrieh, Z. Shokrieh, S.M. Hashemianzadeh, Mater. Des. 64 (2014) 96–101.
[5] A. Yu, P. Ramesh, M.E. Itkis, E. Bekyarova, R.C. Haddon, J. Phys. Chem. C 111 (2007) 7565–7569.
[6] M.Y. Huang, T.A. Pascal, H. Kim, W.A. Goddard, J.R. Greer, Nano Lett. 11 (2011) 1241–1246.
[7] R.J. Young, I.A. Kinloch, L. Gong, K.S. Novoselov, Compos. Sci. Technol. 72 (2012) 1459–1476.
[8] Y. Lee, D. Kim, J. Seo, H. Han, S.B. Khan, Polym. Int. 62 (2013) 1386–1394.
[9] F. Barroso-Bujans, A. Alegria, J.A. Pomposo, J. Colmenero, Macromolecules 46 (2013) 1890–1898.
[10] K. Kalaitzidou, H. Fukushima, L.T. Drzal, Carbon 45 (2007) 1446–1452.
[11] J.S. Bunch, S.S. Verbridge, J.S. Alden, A.M. van der Zande, J.M. Parpia, H.G. Craighead, P.L. McEuen, Nano Lett. 8 (2008) 2458–2462.
[12] Q.H. Zhang, X. Zhao, D.J. Chen, P. Lu, Macromolecules 43 (2010) 2357–2363.
[13] L. Jun, S. Jianxiang, Z. Zijian, W. Youping, Z. Liqun, Nanotechnology 26 (2015) 291003.
[14] W.E. Mahmoud, Eur. Polym. J. 47 (2011) 1534–1540.
[15] J.H. Du, H.M. Cheng, Macromol. Chem. Phys. 213 (2012) 1060–1077.
[16] A.G. Mercader, E.A. Castro, A.K. Haghi, Nanoscience and Computational Chemistry: Research Progress, Apple Academic Press, Oakville, Canada, 2013.
[17] K. Karatasos, Macromolecules 47 (2014) 8833–8845.
[18] C. Lin, Y.T. Liu, X.M. Xie, Aust. J. Chem. 67 (2014) 121–126.
[19] F. Barroso-Bujans, F. Fernandez-Alonso, S. Cerveny, S.F. Parker, A. Alegria, J. Colmenero, Soft Matter 7 (2011) 7173–7176.
[20] Y.-J. Park, S.Y. Park, I. In, J. Ind. Eng. Chem. 17 (2011) 298–303.
[21] C. Wang, L. Feng, H. Yang, G. Xin, W. Li, J. Zheng, W. Tian, X. Li, Phys. Chem. Chem. Phys. 14 (2012) 13233–13238.
[22] F. Barroso-Bujans, F. Fernandez-Alonso, J.A. Pomposo, E. Enciso, J.L.G. Fierro, J. Colmenero, Carbon 50 (2012) 5232–5241.
[23] F. Barroso-Bujans, S. Cerveny, A. Alegria, J. Colmenero, Macromolecules 46 (2013) 7932–7939.
[24] B. Ardeshirzadeh, N.A. Anaraki, M. Irani, L.R. Rad, S. Shamshiri, Mater. Sci. Eng. C Mater. 48 (2015) 384–390.
[25] R.A. Bader, D.A. Putnam, Engineering polymer systems for improved drug delivery, Wiley, Hoboken, New Jersey, 2014.
[26] O. Borodin, G.D. Smith, Molecular modeling of poly(ethylene oxide) melts and poly(ethylene oxide)-based polymer electrolytes, in: L.A. Curtiss, N.S. Gordon (Eds.), Computational Materials Chemistry: Methods and Applications, Kluwer Academic Publishers, Dordrecht 2004, pp. 35–90.
[27] M.-L. Saboungi, D.L. Price, G. Mao, R. Fernandez-Perea, O. Borodin, G.D. Smith, M. Armand, W.S. Howells, Solid State Ionics 147 (2002) 225–236.
[28] W. Wieczorek, D. Raducha, A. Zalewska, J.R. Stevens, J. Phys. Chem. B 102 (1998) 8725–8731.
[29] Y.C. Cao, C.X. Xu, X. Wu, X. Wang, L. Xing, K. Scott, J. Power Sources 196 (2011) 8377–8382.
[30] G. Liu, C. Guan, H. Xia, F. Guo, X. Ding, Y. Peng, Macromol. Rapid Commun. 27 (2006) 1100–1104.
[31] D. Ratna, J. Karger-Kocsis, J. Mater. Sci. 43 (2008) 254–269.
[32] X. Bai, Y. Zhai, Y. Zhang, J. Phys. Chem. C 115 (2011) 11673–11677.
[33] H.B. Lee, A.V. Raghu, K.S. Yoon, H.M. Jeong, J. Macromol. Sci. B 49 (2010) 802–809.
[34] Y.J. Son, Y.H. Park, S.Y. Park, I. In, Chem. Lett. 44 (2015) 542–544.
[35] Y. Matsuo, K. Tahara, Y. Sugie, Carbon 35 (1997) 113–120.
[36] T.N. Abraham, D. Ratna, S. Siengchin, J. Karger-Kocsis, Polym. Eng. Sci. 49 (2009) 379–390.
[37] M.M. Elmahdy, K. Chrissopoulou, A. Afratis, G. Floudas, S.H. Anastasiadis, Macromolecules 39 (2006) 5170–5173.
[38] Q. Jing, W. Liu, Y. Pan, V.V. Silberschmidt, L. Li, Z. Dong, Mater. Des. 85 (2015) 808–814.
[39] F. Barroso-Bujans, F. Fernandez-Alonso, S. Cerveny, S. Arrese-Igor, A. Alegria, J. Colmenero, Macromolecules 45 (2012) 3137–3144.
[40] F. Barroso-Bujans, F. Fernandez-Alonso, J.A. Pomposo, S. Cerveny, A. Alegria, J. Colmenero, ACS Macro Lett. 1 (2012) 550–554.
[41] Y.F. Wang, X.L. Hou, C. Cheng, L. Qiu, X.H. Zhang, G.P. Simon, D. Li, Aust. J. Chem. 67 (2014) 168–172.
[42] Y.K. Godovsky, G.L. Slonimsky, N.M. Garbbar, J. Polym. Sci. C 38 (1972) 1–21.
[43] K. Niedzwiedz, A. Wischnewski, W. Pyckhout-Hintzen, J. Allgaier, D. Richter, A. Faraone, Macromolecules 41 (2008) 4866–4872.
[44] A.S. Wajid, S. Das, F. Irin, H.S.T. Ahmed, J.L. Shelburne, D. Parviz, R.J. Fullerton, A.F. Jankowski, R.C. Hedden, M.J. Green, Carbon 50 (2012) 526–534.
[45] L. Gong, R.J. Young, I.A. Kinloch, I. Riaz, R. Jalil, K.S. Novoselov, ACS Nano 6 (2012) 2086–2095.
[46] X. Jiang, L.T. Drzal, Polym. Compos. 33 (2012) 636–642.
[47] D.W. Van Krevelen, Properties Of polymers their correlation with chemical structure: their numerical estimation and prediction from additive group contribution, third ed. Elsevier Scientific Publishing Company, New York, 1990.
[48] S.J. Weiner, P.A. Kollman, D.T. Nguyen, D.A. Case, J. Comput. Chem. 7 (1986) 230–252.
[49] R. Buscaglia, M.C. Miller, W.L. Dean, R.D. Gray, A.N. Lane, J.O. Trent, J.B. Chaires, Nucleic Acids Res. 41 (2013) 7934–7946.
[50] J.-K. Hyun, H. Dong, C.P. Rhodes, R. Frech, R.A. Wheeler, J. Phys. Chem. B 105 (2001) 3329–3337.
[51] I. Tanis, K. Karatasos, Phys. Chem. Chem. Phys. 11 (2009) 10017–10028.
[52] J.L. Tsai, S.H. Tzeng, Y.J. Tzou, Int. J. Solids Struct. 47 (2010) 503–509.
[53] J.L. Tsai, J.F. Tu, Mater. Des. 31 (2010) 194–199.
[54] F. Scarpa, S. Adhikari, A.S. Phani, Nanotechnology 20 (2009) 065709.
[55] X.C. Zhao, J. Phys. Chem. C 115 (2011) 6181–6189.
[56] W.P. Lv, M.D. Chen, R.A. Wu, Soft Matter 9 (2013) 960–966.
[57] J. Katoch, S.N. Kim, Z.F. Kuang, B.L. Farmer, R.R. Nalk, S.A. Tatulian, M. Ishigami, Nano Lett. 12 (2012) 2342–2346.
[58] L. Martínez, R. Andrade, E.G. Birgin, J.M. Martínez, J. Comput. Chem. 30 (2009) 2157–2164.
[59] W. Humphrey, A. Dalke, K. Schulten, J. Mol. Graphs. 14 (1996) 33–38.
[60] E.P. Bellido, J.M. Seminario, J. Phys. Chem. C 114 (2010) 22472–22477.
[61] S.E. Feller, Y. Zhang, R.W. Pastor, B.R. Brooks, J. Chem. Phys. 103 (1995) 4613–4621.
[62] T. Darden, L. Perera, L. Li, L. Pedersen, Structure 7 (1999) R55–R60.
[63] J. Phillips, R. Braun, W. Wang, J. Gumbart, E. Tajkhorshid, E. Villa, C. Chipot, R. Skeel, L. Kale, K. Schulten, J. Comput. Chem. 26 (2005) 1781–1782.
[64] W. Hu, T. Albrecht, G. Strobl, Macromolecules 32 (1999) 7548–7554.
[65] I.S. Kolesov, R. Androsch, H.J. Radusch, J. Therm. Anal. Calorim. 78 (2004) 885–895.
[66] H. Meyer, F. Müller-Plathe, Macromolecules 35 (2002) 1241–1252.
[67] J.D. Menczel, R.B. Prime, Thermal analysis of polymers. fundamentals and applications, John Wiley & Sons, Inc., Hoboken, New Jersey, 2009.
[68] J.A. Torres, P.F. Nealey, J.J. de Pablo, Phys. Rev. Lett. 85 (2000) 3221–3224.

[69] T. Lucyshyn, G. Knapp, M. Kipperer, C. Holzer, J. Appl. Polym. Sci. 123 (2012) 1162–1168.
[70] D. Walsh, P. Zoller, Standard pressure volume temperature data for polymers, CRC Press, Lancaster, Pennsylvania, USA, 1995.
[71] H. Takeuchi, J. Chem. Phys. 109 (1998) 5614–5621.
[72] G. Strobl, Prog. Polym. Sci. 31 (2006) 398–442.
[73] R.H. Gee, N. Lacevic, L.E. Fried, Nat. Mater. 5 (2006) 39–43.
[74] J. Mark, K. Ngai, W. Graessley, L. Mandelkern, E. Samulski, J. Koenig, G. Wignall, Physical properties of polymers, Cambridge University Press, Cambridge, United Kingdom, 2004.
[75] E. Di Maio, S. Iannace, L. Sorrentino, L. Nicolais, Polymer 45 (2004) 8893–8900.
[76] W. Kai, Y. Hirota, L. Hua, Y. Inoue, J. Appl. Polym. Sci. 107 (2008) 1395–1400.
[77] S. Kinugasa, H. Hayashi, S. Hattori, Polym. J. 22 (1990) 1059–1064.
[78] G.D. Smith, D.Y. Yoon, R.L. Jaffe, R.H. Colby, R. Krishnamoorti, L.J. Fetters, Macromolecules 29 (1996) 3462–3469.
[79] B.K. Annis, M.-H. Kim, G.D. Wignall, O. Borodin, G.D. Smith, Macromolecules 33 (2000) 7544–7548.
[80] V.V. Ginzburg, A.C. Balazs, Macromolecules 32 (1999) 5681–5688.
[81] Y. Li, Polymer 52 (2011) 2310–2318.
[82] M. Yoonessi, J.R. Gaier, Acs Nano, 4 (2010) 7211–7220.
[83] S. Araby, N. Saber, X. Ma, N. Kawashima, H. Kang, H. Shen, L. Zhang, J. Xu, P. Majewski, J. Ma, Mater. Des. 65 (2015) 690–699.
[84] I. Garcia-Yoldi, F. Alvarez, J. Colmenero, J. Chem. Phys. 138 (2013) 094308.
[85] J. Baschnagel, K. Binder, Macromolecules 28 (1995) 6808–6818.
[86] A.N. Rissanou, V. Harmandaris, Macromol. Symp. 331–332 (2013) 43–49.
[87] G. Scocchi, P. Posocco, M. Fermeglia, S. Pricl, J. Phys. Chem. B 111 (2007) 2143–2151.
[88] T. Yamamoto, Polymer 50 (2009) 1975–1985.
[89] J.Z. Xu, T. Chen, C.L. Yang, Z.M. Li, Y.M. Mao, B.Q. Zeng, B.S. Hsiao, Macromolecules 43 (2010) 5000–5008.
[90] K. Chrissopoulou, K.S. Andrikopoulos, S. Fotiadou, S. Bollas, C. Karageorgaki, D. Christofilos, G.A. Voyiatzis, S.H. Anastasiadis, Macromolecules 44 (2011) 9710–9722.
[91] J.-S. Yang, C.-L. Yang, M.-S. Wang, B.-D. Chen, X.-G. Ma, Phys. Chem. Chem. Phys. 13 (2011) 15476–15482.
[92] J.-S. Yang, D.-H. Huang, Q.-L. Cao, Q. Li, L.-Z. Wang, F.-H. Wang, Chin. Phys. B 22 (2013) 098101.
[93] L.z. Wang, L.l. Duan, Comput. Theor. Chem. 1002 (2012) 59–63.
[94] O. Borodin, G.D. Smith, R. Bandyopadhyaya, O. Byutner, Macromolecules 36 (2003) 7873–7883.
[95] A.N. Rissanou, A.J. Power, V. Harmandaris, Polymers 7 (2015) 390–417.
[96] D. Cai, M. Song, Nanotechnology 20 (2009) 315708.
[97] D. Barun, K.E. Prasad, U. Ramamurty, C.N.R. Rao, Nanotechnology 20 (2009) 125705.
[98] Q.H. Yang, C.J. Qian, H. Li, M.B. Luo, Phys. Chem. Chem. Phys. 16 (2014) 23292–23300.
[99] H.X. Guo, X.Z. Yang, T. Li, Phys. Rev. E 61 (2000) 4185–4193.
[100] H. Eslami, F. Muller-Plathe, J. Phys. Chem. B 115 (2011) 9720–9731.
[101] M. Alaghemandi, M.R. Gharib-Zahedi, E. Spohr, M.C. Bohm, J. Phys. Chem. C 116 (2012) 14115–14122.
[102] K.C. Daoulas, V.A. Harmandaris, V.G. Mavrantzas, Macromolecules 38 (2005) 5780–5795.
[103] Y. Gao, J. Liu, L. Zhang, D. Cao, Macromol. Theory Simul. 23 (2013) 36–48.
[104] J. Liu, Y. Wu, J. Shen, Y. Gao, L. Zhang, D. Cao, Phys. Chem. Chem. Phys. 13 (2011) 13058–13069.
[105] B. O'Shaughnessy, D. Vavylonis, J. Phys. Condens. Matter 17 (2005) R63.
[106] C. Batistakis, A.V. Lyulin, M.A.J. Michels, Macromolecules 45 (2012) 7282–7292.
[107] A.N. Rissanou, V. Harmandaris, Macromolecules 48 (2015) 2761–2772.
[108] S. Provencher, Comput. Phys. Commun. 27 (1982) 229.
[109] O.A. Hickey, G.W. Slater, Phys. Lett. A 364 (2007) 448–452.
[110] W.-S. Tung, N. Clarke, R.J. Composto, K.I. Winey, Macromolecules 46 (2013) 2317–2322.
[111] K. Karatasos, D.B. Adolf, S. Hotston, J. Chem. Phys. 112 (2000) 8695–8706.
[112] J.D. Ferry, Viscoelastic Properties of Polymers, John Wiley & Sons, New York, 1980.
[113] J.-S. Gao, S.-C. Shiu, J.-L. Tsai, J. Compos. Mater. 47 (2013) 449–458.